nature neuroscience

# Auto-attraction of neural precursors and their neuronal progeny impairs neuronal migration

Julia Ladewig[1,2], Philipp Koch[1,2] & Oliver Brüstle[1]

**Limited neuronal migration into host brain tissue is a key challenge in neural transplantation. We found that one important mechanism underlying this phenomenon is an intrinsic chemotactic interaction between the grafted neural precursor cells (NPCs) and their neuronal progeny. NPCs secrete the receptor tyrosine kinase ligands FGF2 and VEGF, which act as chemoattractants for neurons. Interference with these signaling pathways resulted in enhanced migration of human neurons from neural clusters.**



Transplantation of neural stem or progenitor cells is an interesting prospect for neuronal replacement in various neurological disorders[1–3]. The efficacy of such transplants will critically depend on efficient migration and integration of donor neurons into the host brain. Neural transplants placed into the adult brain generally form dense clusters at the site of implantation, with only restricted migration of graft-derived neurons into the host brain[4–6]. It has been suggested that migration of transplanted cells might be hampered because the tissue is already fully established, guiding cues are limited and the space is more constricted[7]. In addition, glial scarring at the site of engraftment has been considered to inhibit neuronal migration[8,9]. We hypothesized that graft-intrinsic interactions between NPCs and their neuronal progeny might interfere with neuronal migration.

To test this hypothesis, we used pluripotent stem cell–derived neural precursors expressing GFP from the neuron-specific doublecortin (*DCX*) promoter and studied the migration capacity of GFP$^+$ immature neurons in the context of differentiating NPCs (NPC-diff) and as fluorescence-activated cell sorting (FACS)-purified neuronal population[10,11] (**Supplementary Fig. 1**). *In vitro*, purified neurons spotted on a matrigel scaffold show prominent centrifugal dissemination. In contrast, NPC-diff form spherical clusters with hardly any neuron leaving these aggregates (**Fig. 1a**,**b**). A similar phenomenon was observed in Boyden chamber migration assays. Although 59.8 ± 11.0% of the purified neurons reached the plain media-filled bottom well of the chamber, only 27.7 ± 5.8% of the neurons in the NPC-diff population migrated through the filter (data normalized to the total number of spotted neurons, mean ± s.d., unpaired *t* test, $P < 0.05$, $n = 3$). On hippocampal slice cultures, purified neurons migrated across large areas of the slices in the horizontal and vertical planes (**Fig. 1c**,**d**). In contrast, neurons in the NPC-diff population formed dense clusters at the target site, with only limited penetration of the tissue (**Fig. 1e**,**f**). For detailed quantification, we mixed GFP$^+$ purified neurons with different numbers of unlabeled NPCs (**Supplementary Fig. 2**). We found that an increased number of NPCs substantially correlated with a decreased distribution of GFP$^+$ neurons in the slices. Thus, purified neurons have a pronounced migratory potential, which is constrained in the presence of NPCs.

We next asked whether secretion of chemotactic factors by the NPCs might be responsible for this phenomenon. Consistent with this idea, neurons migrated toward NPCs when exposed in a Boyden chamber assay (**Fig. 2a**). Using the same device, we identified PDGF-AA, FGF2 and VEGF as factors attracting immature neurons (**Fig. 2a**). Quantitative reverse transcription (RT)-PCR revealed pronounced expression of FGF2 and VEGF in NPCs, whereas we found no substantial expression in purified neurons of either of the factors (**Fig. 2b** and **Supplementary Fig. 3a**). However, neurons expressed appropriate receptors (**Supplementary Fig. 3b**). To determine whether FGF2 and VEGF have a true chemotactic versus an undirected chemokinetic effect on immature neurons, we performed Dunn chamber assays[12]. We observed a clear directional migration toward both FGF2 and VEGF (quantified as forward migration index (FMI); **Fig. 2c** and **Supplementary Fig. 3c–g**). This chemotactic effect could be inhibited

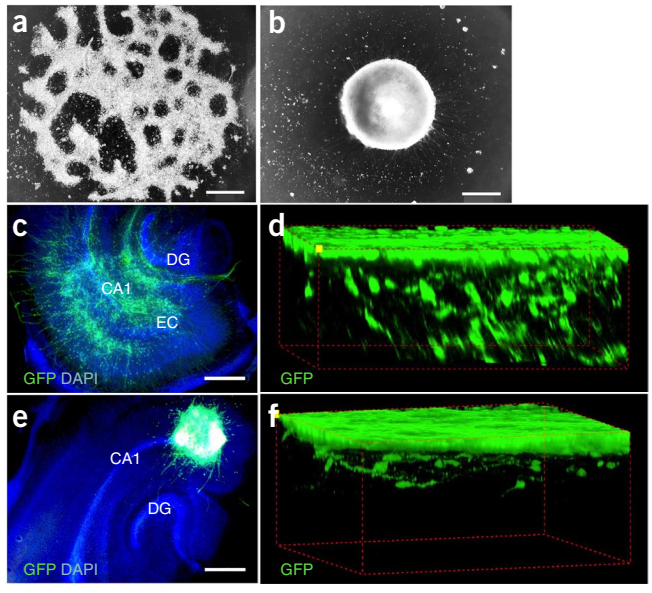


**Figure 1** Purified neurons exhibit a vastly enhanced migration potential. (**a**,**b**) Distribution of purified neurons (**a**) and NPC-diff populations (**b**) on a matrigel scaffold. (**c**–**f**) Distribution of purified neurons (**c**,**d**) and NPC-diff populations (**e**,**f**) on hippocampal slice cultures in the horizontal (**c**,**e**) and vertical planes (**d**,**f**). Scale bars represent 500 μm (**a**,**b**) and 850 μm (**c**,**e**).

[1]Institute of Reconstructive Neurobiology, LIFE and BRAIN Center, University of Bonn and Hertie Foundation, Bonn, Germany. [2]These authors contributed equally to this work. Correspondence should be addressed to O.B. (brustle@uni-bonn.de).

Received 13 September; accepted 24 October; published online 17 November 2013; doi:10.1038/nn.3583

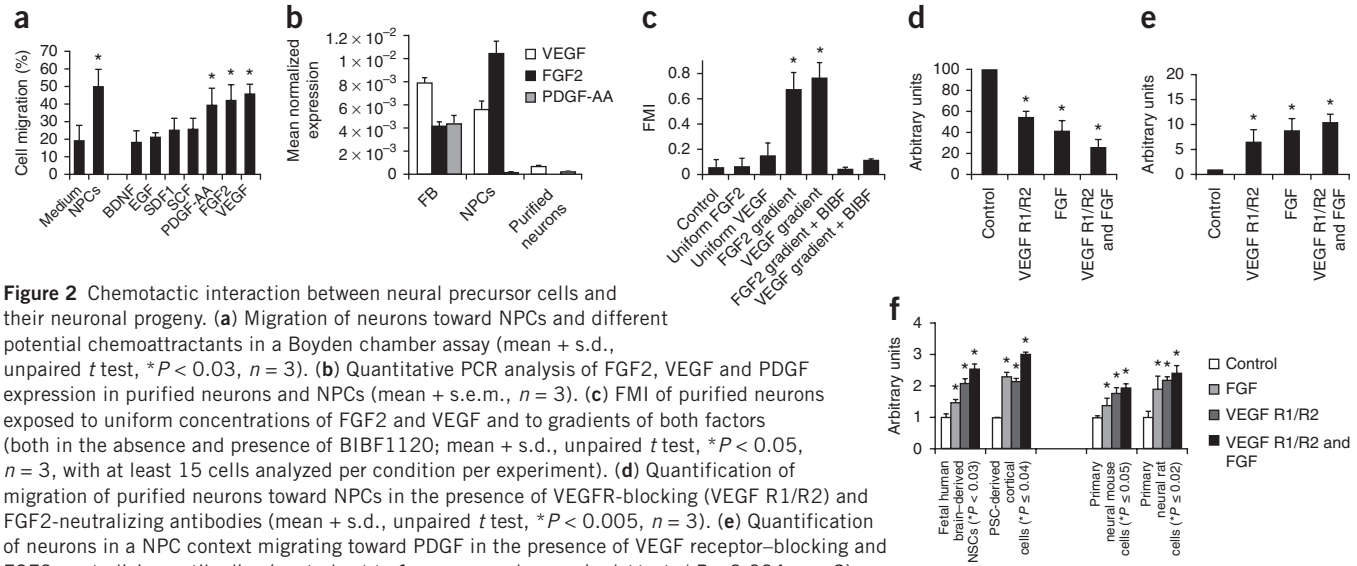


**Figure 2** Chemotactic interaction between neural precursor cells and their neuronal progeny. (**a**) Migration of neurons toward NPCs and different potential chemoattractants in a Boyden chamber assay (mean + s.d., unpaired *t* test, $^*P < 0.03$, $n = 3$). (**b**) Quantitative PCR analysis of FGF2, VEGF and PDGF expression in purified neurons and NPCs (mean + s.e.m., $n = 3$). (**c**) FMI of purified neurons exposed to uniform concentrations of FGF2 and VEGF and to gradients of both factors (both in the absence and presence of BIBF1120; mean + s.d., unpaired *t* test, $^*P < 0.05$, $n = 3$, with at least 15 cells analyzed per condition per experiment). (**d**) Quantification of migration of purified neurons toward NPCs in the presence of VEGFR-blocking (VEGF R1/R2) and FGF2-neutralizing antibodies (mean + s.d., unpaired *t* test, $^*P < 0.005$, $n = 3$). (**e**) Quantification of neurons in a NPC context migrating toward PDGF in the presence of VEGF receptor–blocking and FGF2-neutralizing antibodies (control set to 1, mean + s.d., unpaired *t* test, $^*P < 0.004$, $n = 3$). (**f**) Quantification of neuronal migration in different neural cell populations toward PDGF in the presence of VEGF receptor–blocking and FGF2-neutralizing antibodies (control set to 1, mean + s.d., unpaired *t* test, $n = 3$). All Boyden chamber assays were performed in triplicates per experiment.

by applying the indolinone derivative BIBF1120, a small molecule targeting FGF and VEGF tyrosine kinase receptors[13] (**Fig. 2c** and **Supplementary Figs. 3h,i** and **4**). To further determine the specific role of FGF2 and VEGF in the observed auto-attraction, we performed Boyden chamber assays in which we applied VEGF receptor–blocking antibodies and/or a FGF2 neutralizing antibody. We observed a significant decrease in migration of purified neurons toward NPCs following antibody treatment (**Fig. 2d**). Vice versa, we found a significant increase in the migration of GFP$^+$ neurons out of a cell mixture containing 30% wild-type NPCs toward the chemoattractant PDGF-AA in the presence of the antibodies (**Fig. 2e**). These results suggest that both VEGF and FGF2 are synergistically involved in the autoattraction between both cell types. We next conducted a series of studies to explore whether auto-attraction of neurons and NPCs is a general phenomenon applicable to different neuronal subpopulations and species. Indeed, VEGF and FGF2 antibody treatment led to a pronounced enhancement of neuronal migration in human PSC-derived cortical cells[14], human fetal brain–derived cells[15], and mouse and rat primary neural cells (**Fig. 2f** and **Supplementary Fig. 5**).

We then employed hippocampal slice cultures to explore whether inhibition of this chemoattractive effect can enhance neuronal migration in neural tissue. Purified GFP$^+$ neurons were mixed back with +30% wild-type NPCs and deposited on slices in the presence of BIBF1120 ($n = 24$; **Fig. 3a–e**). In the horizontal plane, BIBF1120-treated neurons showed a twofold increase in migration compared with untreated controls (**Fig. 3a,c**). Along the *z* axis, the number of GFP-positive neurons reaching the mid- and bottom level planes following BIBF1120 treatment increased 2.4- and 7.0-fold,

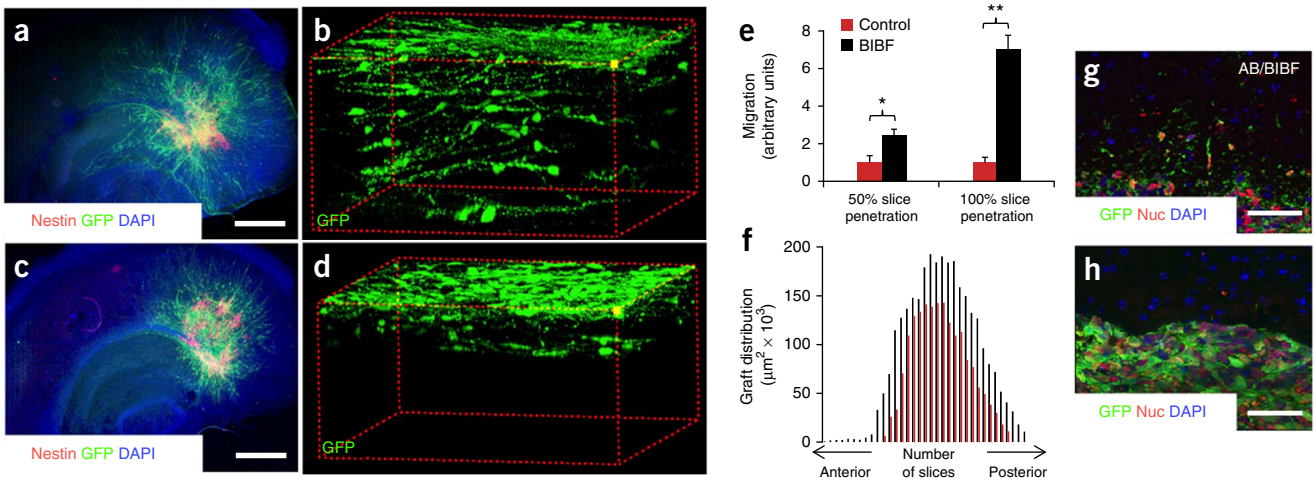


**Figure 3** Inhibition of NPC-neuron auto-attraction results in enhanced migration in CNS tissue. (**a–d**) Distribution of neurons and NPCs on slice cultures in the presence (**a**,**b**) and absence (**c**,**d**) of BIBF1120 in the horizontal (**a**,**c**) and vertical (**b**,**d**) planes. Scale bars represent 850 μm. (**e**) Quantification of vertical slice penetration of GFP-positive neurons (mean + s.d., unpaired *t* test, $^*P < 0.05$, $^{**}P < 0.01$, $n \geq 10$ slices per condition recruited from three independent experiments). (**f**) Anteroposterior spread and graft extension in the coronal plane 1 week following engraftment of NPC-diff cells into the striatum of adult mice with (black) and without (red) exposure to VEGF R1/R2 and FGF2 antibodies and BIBF1120 (AB/BIBF). (**g**,**h**) Representative images of the border of NPC-diff cell grafts derived from antibody and BIBF1120 pretreated (**g**) and untreated (**h**) cells. Scale bars represent 50 μm.

respectively (**Fig. 3b**,**d**,**e**). To study whether inhibition of NPC-neuron auto-attraction can, in principle, enhance migration *in vivo*, we used NPC-diff populations transplanted into the striatum of adult mice. Given that BIBF1120 shows poor blood brain barrier penetration, we pretreated the cells with the blocking and neutralizing antibodies and BIBF1120 and analyzed the graft distribution 1 week after transplantation. We found that pre-treated cells showed a significantly increased anteroposterior spread compared with untreated controls ($1.07 \pm 0.21$ versus $0.63 \pm 0.18$ mm, mean ± s.d., unpaired $t$ test, $P < 0.02$, $n = 12$; **Fig. 3f**). We also detected an increased extension of the grafts in coronal sections. The grafts of the treated cells expanded over a larger area on each single section and showed a less packed structure with more diffuse borders (**Fig. 3f**–**h**). Taken together, our data depict chemoattraction between NPCs and their neuronal progeny as an as yet unrecognized phenomenon and inhibitor of neuronal migration. This mechanism is mediated through receptor tyrosine kinase ligands, applies to a wide range of neural subpopulations from different species, and might serve as a target to overcome limited neuronal migration and tissue integration of neural grafts.

## METHODS

Methods and any associated references are available in the online version of the paper.

*Note: Any Supplementary Information and Source Data files are available in the online version of the paper.*

### ACKNOWLEDGMENTS

We thank J. Itskovitz-Eldor (Technion, Israel Institute of Technology) for providing the human embryonic stem cells (line H9.2) used for generating the neural precursor cells, B. Steinfarz for preparing and culturing the hippocampal slice cultures, A. Leinhaas for support with the *in vivo* experiments, E. Endl at the flow cytometry facility of the University Hospital Bonn for cell sorting, the National Institute of Allergy and Infectious Diseases for contributing the C57BL/10SgSnAi[KO]$\gamma c$-[KO]*Rag2* mice, and J. Tailor and A. Smith (Wellcome Trust-Medical Research Council Stem Cell Institute) for providing human fetal neural stem cells. This work was supported by the European Union (grant 222943 Neurostemcell; LSHG-CT-2006-018739, ESTOOLS), the German Research Foundation (DFG; SFB-TR3) and the Hertie Foundation.

### AUTHOR CONTRIBUTIONS

J.L. and P.K. conceived and designed the study, performed the experiments, assembled, analyzed and interpreted the data, and wrote manuscript. O.B. conceived and designed the study, assembled, analyzed and interpreted the data, and wrote the manuscript.

### COMPETING FINANCIAL INTERESTS

The authors declare competing financial interests: details are available in the online version of the paper.



1. Koch, P., Kokaia, Z., Lindvall, O. & Brustle, O. *Lancet Neurol.* **8**, 819–829 (2009).
2. Lindvall, O. & Kokaia, Z. *Trends Pharmacol. Sci.* **30**, 260–267 (2009).
3. Barker, R.A., Barrett, J., Mason, S.L. & Bjorklund, A. *Lancet Neurol.* **12**, 84–91 (2013).
4. Fricker, R.A. *et al. J. Neurosci.* **19**, 5990–6005 (1999).
5. Roy, N.S. *et al. Nat. Med.* **12**, 1259–1268 (2006).
6. Tabar, V. *et al. Nat. Biotechnol.* **23**, 601–606 (2005).
7. Svendsen, C.N. & Caldwell, M.A. *Prog. Brain Res.* **127**, 13–34 (2000).
8. Kinouchi, R. *et al. Nat. Neurosci.* **6**, 863–868 (2003).
9. Reier, P.J., Perlow, M.J. & Guth, L. *Brain Res.* **312**, 201–219 (1983).
10. Koch, P., Opitz, T., Steinbeck, J.A., Ladewig, J. & Brustle, O. *Proc. Natl. Acad. Sci. USA* **106**, 3225–3230 (2009).
11. Ladewig, J. *et al. Stem Cells* **26**, 1705–1712 (2008).
12. Zicha, D., Dunn, G.A. & Brown, A.F. *J. Cell Sci.* **99**, 769–775 (1991).
13. Hilberg, F. *et al. Cancer Res.* **68**, 4774–4782 (2008).
14. Shi, Y., Kirwan, P., Smith, J., Robinson, H.P. & Livesey, F.J. *Nat. Neurosci.* **15**, 477–486 (2012).
15. Tailor, J. *et al. J. Neurosci.* **33**, 12407–12422 (2013).

## ONLINE METHODS

**Cell culture.** Neural precursor cells derived from human embryonic stem cells (ESCs, line H9.2 passage 32–61) were cultured as described[10]. Lineage selection and FACS of immature neurons was performed as described previously[11]. Differentiation of ESC-derived telencephalic precursor cells was performed according to a reported protocol[14]. In brief, human ESCs were cultured as feeder free monolayer in PluriPro medium (Cell Guidance Systems). Once the cell culture reached 95% confluence, neural induction was initiated by changing the ESC culture medium to neural induction media containing DMEM/F12 (N2 supplement; 1:50), Neurobasal (B27 supplement; 1:50) mixed at a 1:1 ratio and cAMP (300 ng ml$^{-1}$, Sigma-Aldrich), LDN-193189 (0.5 µM, Miltenyi) and A83-01 (0.21 µg, Miltenyi). Cells were maintained in this medium for 8–11 d, collected by dissociation with TrypL Express (Invitrogen) and replated in neural differentiation media containing DMEM/F12 (N2 supplement; 1:50), Neurobasal (B27 supplement; 1:50) mixed at a 1:1 ratio and cAMP (300 ng ml$^{-1}$, Sigma Aldrich) on Geltrex-coated (Life Technologies) plastic dishes for neural differentiation. Differentiation of NSC from human fetal brain was performed along described protocols[15]. For preparation of primary rat and mouse brain cells, pregnant animals were killed (rat E15, strain: CD; mouse E14, strain: NMRI; both from Charles River Laboratories). The embryos were removed and transferred to phosphate-buffered saline (PBS). Subsequently, the embryonic brains were dissected, the meninges, hippocampus and olfactory bulbs were removed, and the cerebral cortices and the ganglionic eminences were prepared in DMEM media (Invitrogen). Tissues were enzymatically digested using 30 U ml$^{-1}$ papain in DMEM for 30–35 min. The digestion was stopped with trypsin inhibitor. The tissue was mechanically triturated to obtain a single-cell suspension and either used directly for Boyden chamber migration assays or plated on poly-l-ornithine/laminin–coated tissue culture dishes (Sigma) for immunofluorescence analysis.

**Matrigel migration assay.** For the matrigel migration assay, the matrigel matrix (BD Bioscience) was thawed at 4 °C overnight and diluted at a ratio of 1:2 in cold DMEM/F12. 250 µl of the matrigel matrix mixture was added per well of a 4-well tissue culture dish and incubated at 37 °C for at least 30 min for hardening. Cells were spotted (1-µl cell suspension containing 100,000 cells in Cytocon Buffer II) on the gel surface, incubated for 10 min at 37 °C for attachment and then covered with differentiation media. The migration of the plated cells was monitored 48 h after plating.

**Boyden chamber migration assay.** The Boyden chamber assay[16] was performed using millicell culture plate inserts (8-µm pore size, Millipore). Cells were plated on the poly-L-ornithine/laminin–coated (both Sigma) membrane that separates the upper and the lower well of the migration chamber. The lower compartment was either filled with media only, with media containing a chemoattractant (30 ng ml$^{-1}$ EGF, BDNF, SDF1, SCF, PDFG-AA, FGF2 or VEGF), or with NPCs, which were plated in the lower well and covered with media before placing the upper well on top. When indicated, VEGF receptor 1 and VEGF receptor 2 blocking antibodies (both R&D Systems; VEGF R1, AF321; VEGF R2, AF357) and the FGF2 neutralizing antibody (Millipore, clone bFM-1) were added at the following final concentrations: 400 ng ml$^{-1}$ VEGF R1 and VEGF R2 antibody, 2 µg ml$^{-1}$ FGF2 neutralizing antibody. When applying different neuronal subpopulations and species (**Fig. 2f**) these contained the following percentages of β-III tubulin–positive neurons: 30–35% cortical PSC-derived populations, 20–25% human fetal brain-derived populations, 55–60% primary mouse cells and 45–50% primary rat cells. After a culture period of 20 h (**Fig. 1**) or 7 h (**Fig. 2**), chambers were fixed with 4% paraformaldehyde (PFA, wt/vol) for 20 min. Either cells on the upper or lower side of the membrane were scraped off. The remaining cells were stained with antibody to GFP or β-III tubulin and counterstained with DAPI before quantification. Data are based on three independent experiments and are shown as mean + s.d.

**Dunn chamber migration assay.** Chemotaxis of immature neurons was directly viewed and recorded in stable concentration gradients of FGF2 (200 ng ml$^{-1}$, R&D) or VEGF (200 ng ml$^{-1}$, R&D) with or without the addition of 2.6 ng ml$^{-1}$ BIBF1120 (stock solution 2 mM in DMSO diluted to 2.4 µM in $H_2O$, Selleck Chemicals) using a Dunn chamber. Chemoattractants added to the outer well of the chamber diffuse across the bridge to the inner well and form a linear steady gradient within ~30 min of loading the chamber[12]. To study chemotaxis, the outer well of the Dunn chamber was filled with medium containing FGF2 or VEGF or medium control, whereas the concentric inner well was filled with medium only. For assessing chemokinesis, the outer and inner wells were filled with equal concentrations of the putative chemoattractant, thereby resulting in a uniform concentration. Coverslips carrying the cultured neurons were inverted and placed onto the chamber. Cell locomotion was recorded through the annular bridge between the concentric inner and outer well over a period of 6 h using a Zeiss Axiovert 200 microscope equipped with a 20× objective. Time-lapse recordings were acquired every 2 min using a ProgResC14 camera (Jena Optic) and Openlab software (Improvision). The cells were kept at 37 °C, 5% $CO_2$ and saturated air humidity.

Directionality of cell movement was analyzed using scatter diagrams of cell displacement. The diagrams were orientated so that the position of the chamber was vertical (*y* direction). Each point represents the final position of the cell at the end of the recording period where the starting point of migration is fixed at the intersection of the two axes. To determine the efficiency of forward migration during a 6-h recording period, the FMI was calculated as the ratio of forward progress to the total path length[17]. Data are based on three independent experiments. For each experiment, 15 cells were randomly picked in the migration region of the chamber and analyzed. Data are shown as mean ± s.d.

**Cytotoxicity, cell viability and differentiation assays.** The CytoTox-ONE homogeneous membrane integrity assay and the CellTiter-Glo luminescent cell viability assay (both Promega) were applied following the supplier's instructions. The cells were incubated with or without 2.6 ng ml$^{-1}$ BIBF1120 for 24 h in case of the cytotoxicity assay and for 4 d in case of the viability assay. For assessing a potential differentiation-promoting effect of BIBF1120 on NPCs, NPCs were cultured in neuronal differentiation medium with or without 2.6 ng ml$^{-1}$ BIBF1120. After 10 d, the percentage of neurons was determined by immunofluorescence using an antibody to β-III tubulin.

**Hippocampal slice culture migration assays.** Hippocampal slice cultures, a suitable model for assessing migration and integration of neural cells in a tissue context under *in vitro* conditions[18] were prepared as described[18,19]. 5–7 d after explantation, 0.5 µl of a cell suspension containing 50,000 cells of either purified neurons or *DCX-GFP* NPCs pre-differentiated for 8 ± 1 d (NPC-diff) were spotted onto the entorhinal cortex of the slice using an injection device.

For studying the interaction between NPCs and immature neurons, 50,000 GFP-positive purified neurons were mixed with 25,000 (+50%), 20,000 (+40%), 15,000 (+30%), 10,000 (+20%), 5,000 (+10%) or 2,500 (+5%) wild-type NPCs in 0.5 µl. 0.5 µl of these mixed cell suspensions were deposited on the entorhinal cortex of the slice cultures.

For kinase inhibition experiments, 50,000 GFP-positive purified neurons were mixed with +30% wild-type NPCs per 0.5 µl, pre-incubated for 30 min with or without 2.6 ng ml$^{-1}$ BIBF1120 (Selleck Chemicals) before spotting 0.5 µl of this cell suspension on the entorhinal cortex ($n$ = 24, recruited from three independent experiments with a minimum of three slices per experiment per condition). The slices were further cultured for 7 d, and 2.6 ng ml$^{-1}$ BIBF1120 was applied every day to the slice media.

Migration was monitored 7 d following transplantation after fixing the slice cultures in 4% buffered PFA for 4 h and subsequent immunohistological staining with an body to GFP and Nestin. GFP-positive neurons, which had migrated into the 400-µm-thick slice tissue were quantified in 10-µm-thick optical planes cut through the mid and bottom level of the slice using the AxioImager.Z1 microscope and AxioVison software (Zeiss). In the *x*-*y* plane, we quantified the neurons, which were found in the top 10 µm of the slice outside a 250-µm perimeter around the deposition site. In case of the transplanted purified neurons, no nestin-positve donor cell cluster was discernible; thus, these transplants were quantified in the vertical plain only.

Confocal images for three-dimensional reconstruction were taken with an Olympus IX81 confocal microscope and FV10-ASW software (Version 01.07, Olympus). All data are based on three independent experiments, with at least three analyzed slices per condition per experiment. Data are shown as mean ± s.d.




doi:10.1038/nn.3583

***In vivo* transplantation into the adult rodent brain.** For experiments in which FGF2 and VEGF signaling was inhibited *in vivo*, NPC-diff (100,000 cells per µl) were trypsinized and either resuspended in transplantation buffer containing 25 ng $\mu l^{-1}$ VEGF R1 and VEGF R2 blocking antibody, 125 ng $\mu l^{-1}$ FGF2 neutralizing antibody and 1.25 µg $\mu l^{-1}$ BIBF1120 or in transplantation buffer only. 1 µl of cell suspension was grafted into C57BL/6 *Rag2*$^{-/-}\gamma^{-/-}$ mice (C57BL/10SgSnAi[KO]$\gamma c$-[KO]*Rag2* (ref. 20); coordinates: anteroposterior 0.7 mm, mediolateral 2 mm, ventral 3 mm). 7 d after transplantation, the recipients were anesthetized and perfused. The brains were removed and cryoprotected in 15% sucrose (wt/vol) in PBS over night, followed by 30% sucrose in PBS for 2 d. Immunofluorescence analysis was performed to identify engrafted human cells in 30- or 40-µm cryosections. Anteriorposterior spread of grafted NPC-diff cells was studied by assessing the presence of human nuclei-positive cells in 40-µm serial coronal sections in five control grafts and seven AB/BIBF grafts. Transplant extension in the coronal plane was measured by quantifying continuous GFP-positive graft areas with a minimum size of 500 $\mu m^2$ in three control and five AB/BIBF striatal grafts using ImageJ64 software. All animal procedures conducted in this study were approved by Landesamt für Natur, Umwelt und Verbraucherschutz Nordrhein-Westfalen.

**Reverse transcription polymerase chain reaction (RT-PCR).** Triplicate total mRNA samples were isolated using an mRNA extraction kit (Qiagen), following the supplier's instructions. 1 µg of total mRNA were used for reverse transcription with the iScript cDNA synthesis kit (Bio-Rad) following the manufacturer's protocol. Semiquantitative PCR reactions were run in at least triplicates using Taq Polymerase (Invitrogen). PCR conditions and cycle numbers were then adjusted to each primer pair for specific DNA amplification on commercially available human fetal brain tissue (single donor, female, 19 weeks of gestation). All reactions were performed on a T3 Thermocycler (Biometra). Quantitative RT-PCR analyses were performed in triplicates on a Bio-Rad iCycler using SYBRI-green detection method. PCR products were assessed by dissociation curve and gel electrophoresis. Data were normalized to GAPDH rRNA levels. Primers used are listed in **Supplementary Table 1**.

**Immunofluorescence.** Cells were fixed in 4% PFA for 20 min at 20–25 °C and permeabilized with 0.1% Triton X-100 (vol/vol, Sigma-Aldrich) in PBS for 20 min. Blocking was performed with 10% fetal calf serum (FCS, vol/vol, Invitrogen) in PBS with 0.1% Triton X-100 for 1 h. Samples were incubated with primary antibodies diluted in blocking solution at 20–25 °C for 3–4 h, washed twice in PBS and incubated with secondary antibody diluted in blocking solution for 45 min, counterstained with DAPI and mounted with vectashield mounting solution (Vector Laboratories). Tissues were stained by permeabilizing/blocking them for 2 h with 0.1% Triton X-100 in PBS containing 10% FCS. Incubation with primary antibodies was for 16 h at 20–25 °C. Washing in PBS was performed for 4 h at 20–25 °C. Incubation with fluorophore-conjugated secondary antibodies was for 2 h at 20–25 °C. For information about antibodies used in this study, see **Supplementary Table 2**.

**Statistical analyses.** Quantitative data was generated at least in biological triplicates. No statistical methods were used to pre-determine sample sizes, but our sample sizes are similar to those generally employed in the field. All data were collected and processed randomly. Two independent people analyzed the data of the Boyden chamber assays (one person blinded) and the average was built. Data distribution was assumed to be normal, but this was not formally tested. Means and s.d. were computed. All results presented as bar graphs show mean + s.d. or + s.e.m. as indicated. Student's *t* test was performed to determine whether a significant difference exists between groups.

16. Richards, K.L. & McCullough, J. *Immunol. Commun.* **13**, 49–62 (1984).
17. Foxman, E.F., Kunkel, E.J. & Butcher, E.C. *J. Cell Biol.* **147**, 577–588 (1999).
18. Opitz, T., Scheffler, B., Steinfarz, B., Schmandt, T. & Brustle, O. *Nat. Protoc.* **2**, 1603–1613 (2007).
19. Scheffler, B. *et al. Development* **130**, 5533–5541 (2003).
20. Cao, X. *et al. Immunity* **2**, 223–238 (1995).